ANNALS OF GEOPHYSICS, 66, 6, SE643, 2023; doi:10.4401/ag-8901
OPEN ACCESS

Space-based GNSS radio signals to investigate ionospheric plasma changes preceding the 2016 Al Hoceima-Morocco earthquake, Mw = 6.4

Abdennasser Tachema[*,1], Abdelmansour Nadji[2], Deepak Kumar Sondhiya[3]

(1) Institute of Science and Applied Techniques, Department of Science, University of Tlemcen, 13000 Tlemcen, Algeria
(2) Research Laboratory: Géoressources, Environnement et Risques Naturels (GEOREN), University of Oran 2, Mohamed Ben Ahmed, Faculty of Earth Sciences and the Universes, 31000 Oran, Algeria
(3) School of Sciences, SAGE University, Bhopal, India

Article history: received August 24, 2023; accepted November 27, 2023

Abstract

This paper examines abrupt variations in ionospheric electron density preceding the Al Hoceima earthquake (January 25th, 2016, Mw = 6.4, Northern Morocco). The observed anomalous behavior in the F2-ionospheric region, at about 350 km altitude, raises the possibility of a connection with impending seismic activity of moderate-to-great magnitude, supporting the hypothesis that Total Electron Content (TEC) variations could serve as potential earthquake precursors. For this purpose, we have exploited one of the main ionospheric keys, TEC, through a network of over one hundred dual-frequency Global Positioning System/Global Navigation Satellite Systems (GPS/GNSS) receivers. Through calculation algorithms based on spherical harmonic analysis of GPS/GNSS Observation-Navigation data, we were able to produce local ionospheric maps to restore the GPS-TEC signal and investigate potential ionospheric disturbances associated with this shallow-focus and strong earthquake.

Since the ionospheric TEC is a function of the variability and dynamics of the Earth's ionosphere, mainly time-space and solar-geomagnetic activities, we had to consider each of these disturbing factors separately. In fact, the seismic zone of Al Hoceima (Morocco, North Africa), at about 35°N latitude, belongs to the region of low geographical latitudes. In such regions the variations of the ionospheric layer are slight. Moreover, during the earthquake preparation period, space weather conditions exhibited a calm state characterized by low solar activity and the absence of geomagnetic storms. The adequate effects of these physical conditions allow us, through wavelet transform, to emerge solely signatures of earthquake-related ionospheric disturbances. Based on the seismo-ionospheric combination model, we have highlighted some ionospheric electron density irregularities that decreased abnormally, near the epicenter several days prior to the 2016 Al Hoceima main event. From these findings, we can state that such research provides a promising approach for predicting earthquakes through large fluctuations in the ionized shell of the Earth's atmosphere, thereby offering the prospect of a life-saving seismic alarm.

Keywords: Al Hoceima-Morocco earthquake 2016; Ionospheric Total Electron Content; Pre-seismic signatures in ionosphere; Seismo-ionospheric combination model; Wavelet transform; Spherical harmonic analysis

1. Introduction

Earthquakes are considered one of the most destructive and damaging natural phenomena on the globe, so predicting their occurrence seems to be a crucial issue. Since the mid-20th century, considerable efforts have been made in short-term earthquake prediction to reduce the loss of human life and material damage [Coburn and Spence, 2002].

In this context, numerous studies have explored the possible relationship between pre-earthquake processes and ionospheric disturbances, where the outcomes achieved from the majority of these works have shown the possibility of predicting the occurrence of these phenomena over a time period ranging from minutes to days. As a key prediction indicator, it is worth mentioning the fluctuations in the ionospheric electron density and total electron content (TEC[1]) governed by dynamic coupling: solid Earth and its atmospheric envelope [Liu et al., 2000, 2009; Tachema and Nadji, 2019, 2020; Sasmal et al., 2021; Tachema, 2022; Tachema et al., 2022]. In-depth investigations of these pre-earthquake ionospheric fluctuations, using satellite-based radionavigation systems, have recently become an area of great interest to several research laboratories and scientists worldwide. Most such studies reveal abrupt enhancement or depletion in the time series of the ionospheric TEC, appearing before the arrival of the main shocks. To name a few, Liu et al. [2009] found that the free electron content over the epicentral region decreased and increased in the late evening and afternoon, respectively, on the days preceding the major earthquake in Wenchuan, China, during the spring of 2008. After selecting ionospheric data under quiet geomagnetic conditions, Satti et al. [2022] statistically identified pre-seismic ionospheric anomalies associated with two large magnitude earthquakes ($Mw \geq 6.5$) in the USA and Turkey. Similarly, Sekertekin et al. [2020] thoroughly analyzed ionospheric TEC data via the moving median method, and identified anomalous TEC enhancement-depletion (imminent seismo-ionospheric precursors) a few days before the 2013 Awaran-Pakistan Mw 7.7 earthquake.

Amidst this body of research, which suggests the possible emergence of ionospheric anomalies preceding substantial earthquakes, the scientific community has also engaged in deliberations and inquiries questioning these connections. Notable among these discussions are the studies conducted by Dautermann et al. [2007] and Thomas et al. [2017]. These investigations have probed the potential correlation between variations in TEC and seismic events. In this context, the current study holds importance as a targeted case that reinforces the broader hypothesis of connections between TEC and seismic activity, while also contributing to the ongoing discussion about potential links between ionospheric dynamics and seismic events.

It should be noted that the identification of anomalous changes in the TEC parameter before notable earthquakes ($M \geq 5$) requires a complete understanding of the connection between ionospheric processes and seismic occurrences. In this present work, we investigate the TEC behavior preceding the shallow-focus (10-12 km) and strong earthquake ($Mw = 6.4$) that struck the Moroccan city of Al Hoceima on January 25th, 2016. The epicenter was located in the western Mediterranean near the coast of the Alboran Sea. For this purpose, the GPS/GNSS dataset used to identify the seismo-related signatures in the Earth's ionized atmosphere was processed over a period of two consecutive months. These geodetic data consist of observation and navigation messages files archived in the standard Receiver Independent Exchange (RINEX), files format. They are sourced from the worldwide network of permanent GNSS receivers, with daily 30-second sampling rates available through the official website of the International GNSS Service (IGS). In order to analyze the ionospheric TEC profile and track changes, we have implemented an algorithm generating daily 2-hour time intervals of ionospheric maps. Employing spherical harmonic analysis, we constructed thematic cartography of free electrons in the upper part of the Earth's atmosphere (approximately 350 km altitude), enabling the determination of ionospheric TEC irregularities occurring a few days in advance of the 2016 $Mw = 6.4$ Al Hoceima earthquake mainshock.

1 Refers to the number of electrons present in a column of the Earth's ionosphere and is expressed in TEC units (TECU). 1 TECU = 10^{16} electrons/m^2.

2. Al Hoceima-Alboran Ridge earthquake, January 25th, 2016 (Mw = 6.4)

On 25 January 2016 at 04h 22mn 01sc UTC/LT time, a shallow and strong earthquake (Mw = 6.4) occurred in the offshore area of northern Morocco (40 km NNE of Al Hoceima city, 35.6004° N, 3.8056° W), as shown in Figure 1. It is reportedly the largest since the 2004 Al Hoceima earthquake, along the Moroccan-Iberian section of the African-Eurasian plate boundary. A comprehensive assessment of different earthquake catalogs, namely IGN[2], USGS[3], IRIS[4] and INGV[5], affirms the heightened seismic proneness of the northern Moroccan margin compared to the western expanse bordering the Atlantic Ocean.

2.1 Seismotectonics of the Alboran region and vicinity

The Al Hoceima region is geographically located near the eastern termination of the Alpine Rif mountain belt and is characterized as the most seismically active area in Morocco [Ben Sari, 2004; Stich et al., 2005]. This region of northern Morocco is situated between two major left-lateral strike-slip faults, the Jebha fault striking N70° and the Nekor fault striking N50°, with NE-SW orientation [Bezzeghoud and Buforn, 1999; Tahayt et al., 2009]. For the period 1900-2021, the seismic event recording instruments show that the vast majority of earthquakes that occurred in Morocco are located in the Al Hoceima region. The seismic catalogs count four shallow (> 15 km) and moderate-to-strong earthquakes ($M_w \geq 5.5$) that struck this zone: Mw = 6.4 (Jan. 25, 2016), Mw = 6.4 (Feb. 24, 2004), Mw = 6.0 (May 26, 1994) and M5.5 (Aug. 23, 1959).

Time [GMT]	Latitude [degree]	Longitude [degree]	Depth [km]	Region	Source
Foreshock 21/01/2016 (Mw = 5.1)					
13:47:19	35.6385	−3.7951	10	South Alboran	IGN
13:47:19	35.625	−3.650	10	Strait of Gibraltar	USGS
Mainshock 25/01/2016 (Mw = 6.4)					
04:22:01	35.6004	−3.8056	12	South Alboran	IGN
04:22:02	35.6493	−3.6818	12	Strait of Gibraltar	USGS
04:22:00	35.50	−3.71	10	Strait of Gibraltar	INGV

Table 1. Information about the 2016 Al Hoceima earthquake from different seismological agencies.

As per the formula introduced by Dobrovolsky et al. [1979], the earthquake preparation zone extends to a radius of 565 km; thereby demonstrating the significant scale of this seismic event.

2 Instituto Geográfico Nacional, http://www.ign.es/web/ign/portal/sis-catalogo-terremotos

3 United States Geological Survey, https://earthquake.usgs.gov/earthquakes/search/

4 Incorporated Research Institutions for Seismology, http://ds.iris.edu/ieb/

5 Istituto Nazionale di Geofisica e Vulcanologia, http://rcmt2.bo.ingv.it/

Figure 1. Distribution of aftershocks epicenters ($3 \leq Mw \leq 6.4$) for the period: January 25th, 2016 to July 25th, 2016 taken from the Spanish Instituto Geográfico Nacional Data File.

3. Data collection and processing

3.1 Permanent GPS/GNSS network

For the purpose of this research, a sample of over one hundred GPS/GNSS stations (see Fig. 2) was meticulously selected in order to compute local vertical TEC measurements and generate two-dimensional TEC mapping. The GPS receivers continuously provide data, sampled at 30-second intervals, in the RINEX files format. Indeed, the geodetic processing of these datasets allowed us to produce grid-based GPS-TEC maps over the Al Hoceima epicentral zone with high temporal (2 hours) and spatial ($\Delta\lambda = 5°$ in longitude direction, $\Delta\varphi = 2.5°$ in latitude direction) resolution.

3.2 Regional-Scale TEC Mapping

Ionospheric mapping, over a 24-hourly time period, using its physical parameter TEC has become an important and reliable tool for monitoring the ionized part of Earth's upper atmosphere. To achieve this, we have used Matlab-based geodetic routines (see diagrammatic representation in Fig. 3) to process RINEX Observation/Navigation files collected from about one hundred permanent stations belonging to the IGS (International GNSS Service) and ERGNSS/IGN (Estaciones de Referencia GNSS/Instituto Geográfico Nacional, Spain) geodetic networks (detailed in Appendix A: Table A1). Sample representations of the local ionospheric TEC variation during the most geomagnetically disturbed and quiet days (http://wdc.kugi.kyoto-u.ac.jp/qddays/format.html), over the epicentral area of the 2016 Al Hoceima earthquake, are illustrated in Figure 4.

It should be noted that the large coverage of dual-frequency GPS/GNSS receivers around the study area provided us a high-resolution mapping of ionospheric total electron content. Thus, the set of two-dimensional TEC maps (generated at 2-hour interval, spanning the region: 33°N-38°N and 9°W-1°W) shows the diurnal and nocturnal variations in the ionospheric layer during both quiet (03.01.2016, DOY 003) and disturbed (20.12.2015, DOY 354) ionospheric days. Higher TEC values indicate a denser ionosphere, while lower TEC values indicate a less dense ionosphere. As shown in Figure 4, we refer to specific dates and times when the ionosphere was either quiet or excited. On January 3rd, 2016 at 16H, the ionosphere was in a quiet-day state, indicative of a relatively lower level of ionization. Conversely, on December 20th, 2015 at 16H, the ionosphere was in an excited-day state, meaning that it was in a higher level of ionization. Indeed, geomagnetic disturbances can lead to alterations in the Earth's magnetic field, consequently impacting the ionospheric layer.

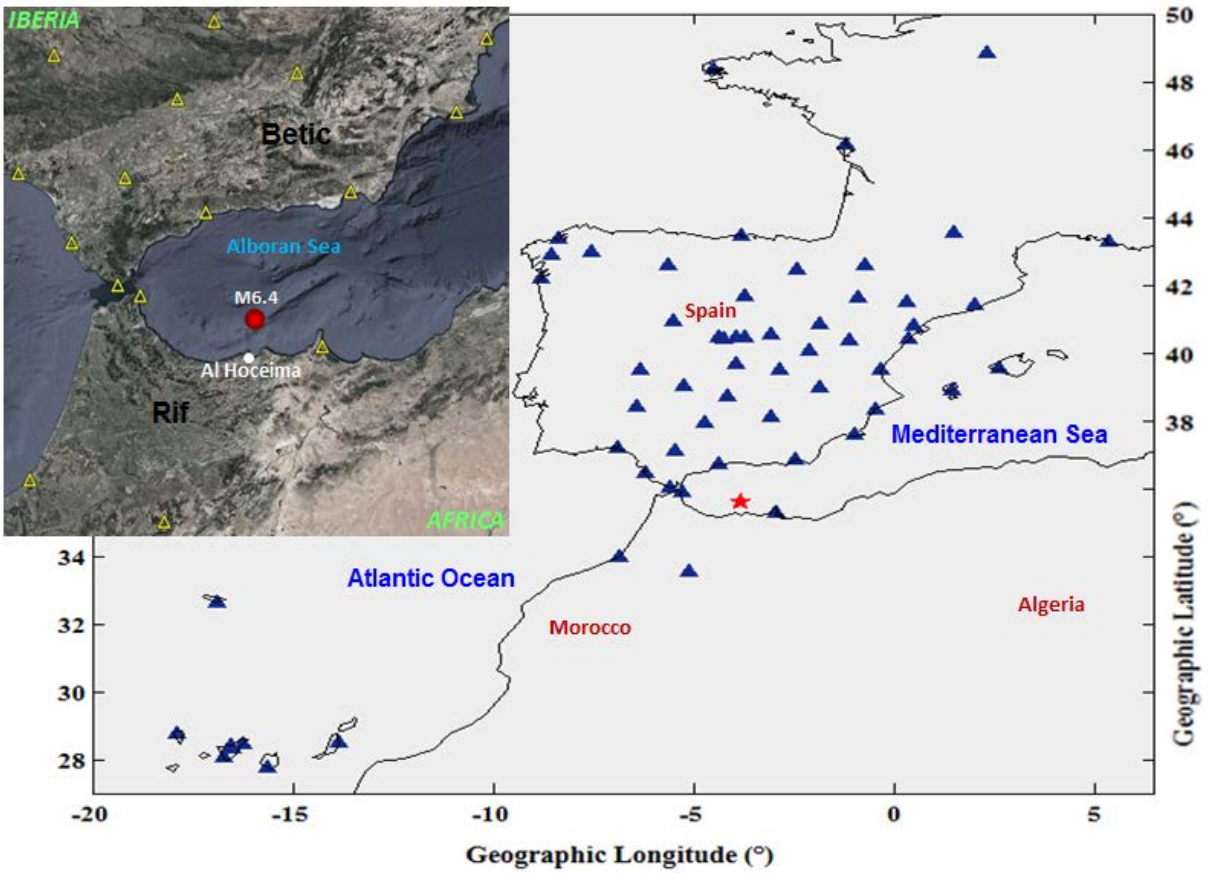

Figure 2. Location of permanent IGS and IGN observation sites, inset shows the epicenter of the offshore 2016 Al Hoceima earthquake belonging to the active axe: Rif Mountains (Morocco)–Alboran–Betic Cordillera (Spain). The epicenter of the January 25th, 2016 (Mw = 6.4) Al Hoceima earthquake is marked by a red star.

This paper's approach to modeling the electron content of the ionospheric F2 region is based on the concept of the thin ionospheric shell (Single Layer Model) situated at an altitude of 350 km above the ground, where the density of free electrons in the ionosphere peaks [Wielgosz et al., 2003; Teunissen and Montenbruck, 2017]. Based on spherical harmonic functions [Hofmann-Wellenhof and Moritz, 2005], the GPS_TEC measurement approach for detecting seismo-ionospheric precursors is summarized in the following flowchart.

Before initiating the process of extracting free electron content, it is necessary to conduct the geodetic data processing for the IGS and ERGNSS networks, encompassing a total of 103 permanent dual-frequency ground-based stations. This geodetic data pre-processing phase involves the following steps:

- Reading the approximate positions of the GPS/GNSS permanent receivers, in Cartesian coordinates (X, Y, Z), provided by the RINEX Observation-files.
- Transformation of Cartesian coordinates into Geographical coordinates (Longitude, Latitude, and Height).
- Reading: RINEX headers, 30s sampled GPS/GNSS observation data (RINEX O-Files) and navigation-ephemeris messages (RINEX N-Files).
- Parameters (coefficients) estimation of the spherical harmonic expansion of the ionospheric model, using the least squares estimator. In this paper, the maximum spherical harmonic degree (and order) of these coefficients is set at 5 and the origin coordinates of the local TEC model (λ_0, φ_0) correspond to the Al Hoceima earthquake epicenter (35.6004° N, 3.8056° W).
- Estimation of GPS/GNSS satellite and receiver differential code biases (assumed constant values), clock biases (by forming single and double differences) as well as variance-covariance matrix calculation (precision on the coefficients).
- Computation of: Geometry-free linear combination of dual-frequency GPS/GNSS code observations, IPP position (intersection between the line of sight satellite-receiver and the ionospheric shell at 350 km altitude), azimuth, and geocentric positions of the satellites.

- Estimation of the vertical distribution of electron density within the ionosphere from the slant measurement, using mapping function approach (SLM obliquity factor).
- Finally, generation of two-dimensional ionospheric maps (TEC Mapping).

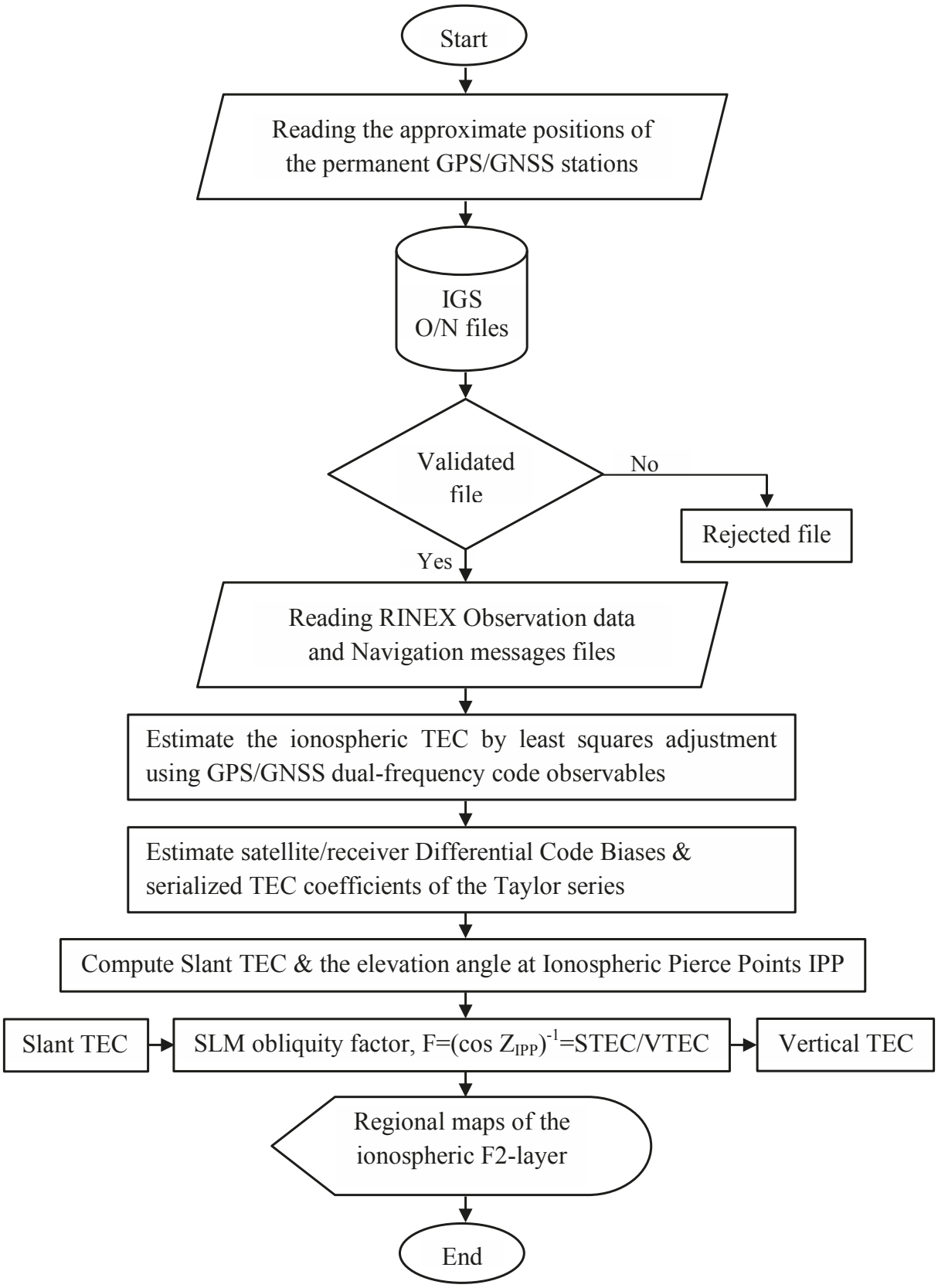

Figure 3. Flowchart of regional ionospheric TEC mapping based on spherical harmonic analysis.

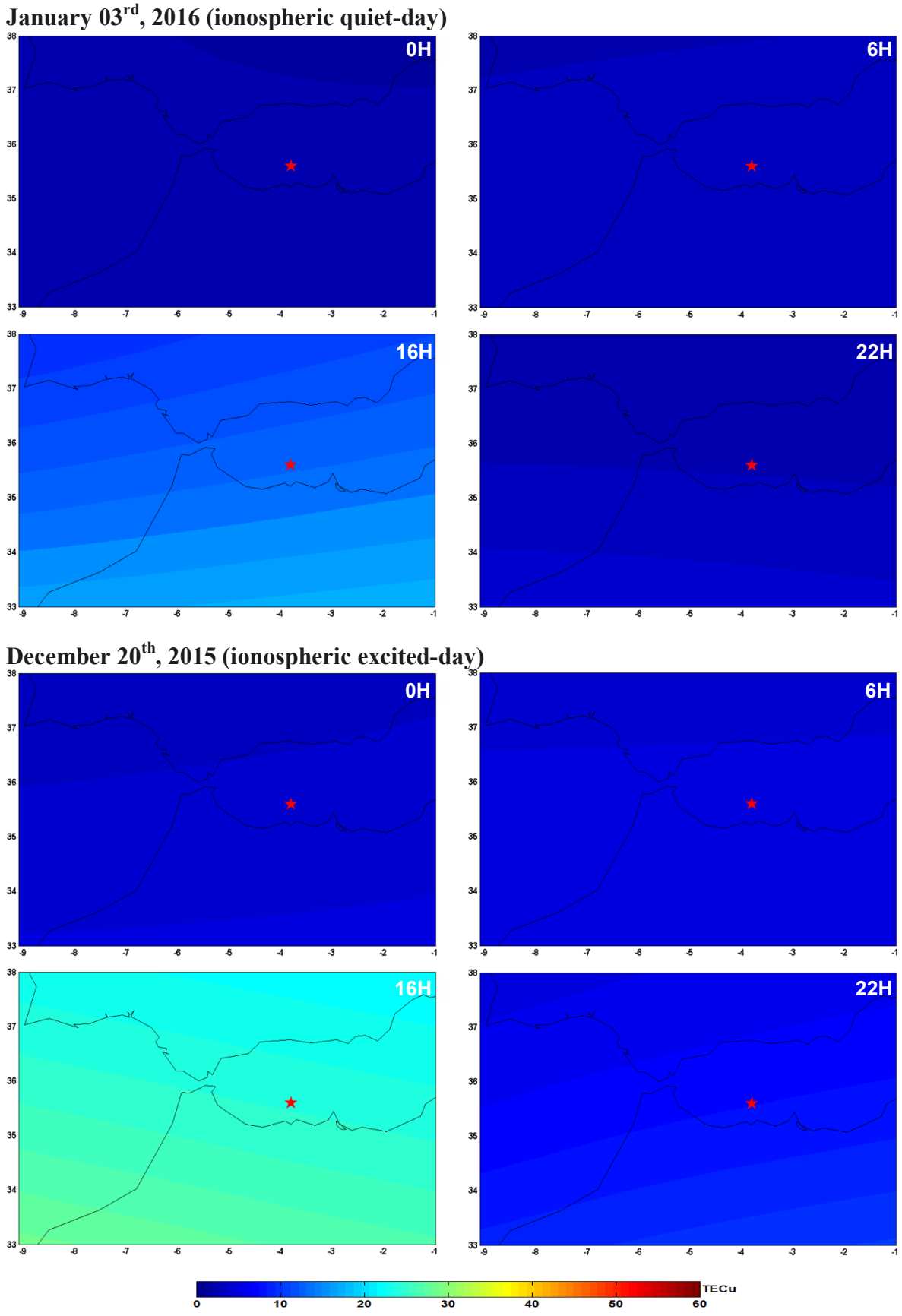

Figure 4. Spatio-temporal variability of the ionospheric F2-layer around the epicentral area (Alboran Sea) of the Al Hoceima-Morocco seismic event. The epicenter of the earthquake is marked by the red star. The local ionospheric TEC maps display both the quietest (03.01.2016) and moderately disturbed (20.12.2015) ionospheric days. Geographic longitudes and latitudes are respectively figured on the X-axis and Y-axis.

The maps in Figure 4 provide a visual representation of the spatio-temporal distribution of ionospheric total electron content for both geomagnetically disturbed and quiet days. The color scale indicates the ionospheric TEC values, where red signifies the uppermost values and shades of blue correspond to the lowest values. These sample maps show that the ionospheric layer is more homogeneous on quiet days, with TEC values distributed evenly across the map. While on geomagnetically disturbed days, larger variations in TEC values are observed across the map, indicating a more complex and disturbed ionosphere. Such information is crucial to highlight the ionosphere's sensitivity to changes in the geomagnetic field, providing a valuable tool for distinguishing the precursors caused by earthquakes from those caused by space weather effects. Therefore, understanding the interplay between geomagnetic and ionospheric activity assumes significance in the accurate interpretation of seismo-ionospheric precursors.

4. Results and discussions

In this section, we aim to identify possible seismo-ionospheric precursors related to the shallow-focus and strong earthquake (Mw = 6.4) that struck Al Hoceima. Noting that this seismic event occurred in the early morning of January 25th, 2016 in the Alboran Sea near the Moroccan coast, precisely at the geographical position of –3.8056° Longitude and 35.6004° Latitude.

4.1 Local pre-seismic ionospheric instabilities

To determine unusual ionospheric variations preceding the 2016 Al Hoceima seismic event, several steps are required (the diagram provided in Figure 3 gives more details on these steps). It is noteworthy that the ionospheric TEC data at the precise location of the earthquake epicenter were retrieved by implementing the interpolation methodology described by Schaer [1999]. This entails computing a weighted average of the four nearest TEC values, a method well-suited for generating highly dense interpolation grids.

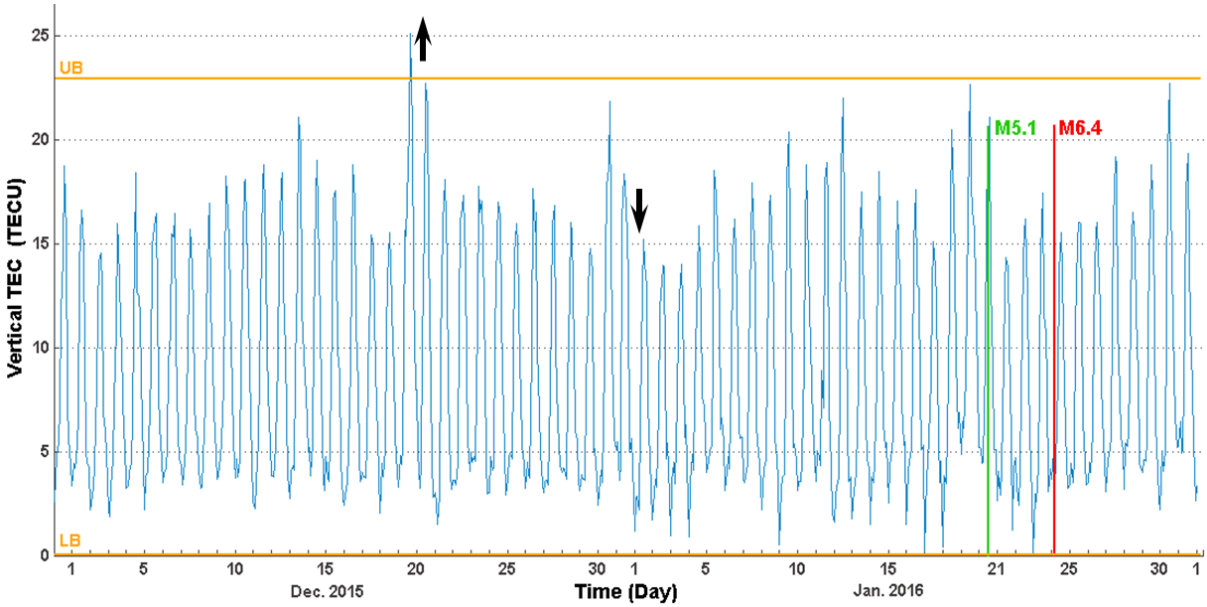

Figure 5. Time series of vertical ionospheric TEC changes observed over the Mw = 6.4 Al Hoceima earthquake epicenter (35.6004° N, 3.8056° W), from December 01st, 2015 to February 01st, 2016. The green and red vertical lines, respectively, indicate the moments of the foreshock (January 21st, 2016, Mw = 5.1, see Table 1) and the main earthquake event (January 25th, 2016, Mw = 6.4). The horizontal limits correspond to the Upper and Lower Bounds using the IQR method. While the black arrows highlight extreme variations in TEC values, where a transiting phase can be visually observed at the beginning of January 02nd, 2016.

The curve chart below represents the GPS vertical ionospheric TEC measurements recorded over the Al Hoceima earthquake preparation zone, through the global GPS/GNSS and the Spanish local ERGNSS geodetic networks.

As can be seen in this line graph, Fig. 5, many TEC perturbations expressed by abrupt peaks and decreases were manifested before the Al Hoceima seismic event. To discern ionospheric TEC values that lie outside the overall pattern in the GPS-TEC distribution, we applied the interquartile range (IQR) statistical method:

$$\begin{cases} Upper_{bound} = Q3 + 1.5 * IQR \\ Lower_{bound} = Q1 - 1.5 * IQR \end{cases} \quad (1)$$

where IQR is the difference between the lower (first, Q1) and the upper (third, Q3) quartiles of the dataset [Dekking et al., 2005]. Here, the dataset are the ionospheric VTEC values along the studied time series. Thus, the TEC value corresponding to the date of December 20th, 2015 is considered abnormal as it falls above the adopted fences.

It should be noted that the ionospheric layer undergoes multiple variations, which are mainly due to the Earth's rotation (diurnal variation), the geographical position (latitudinal variation) as well as the large-scale solar magnetic field of the solar cycle variation [Mitra, 1974; Kelley, 2009; Opio et al., 2015]. This research focuses on examining changes in electron density within the ionospheric F2-layer preceding seismic events in the Earth's lithospheric structural region. However, before we can confirm whether these ionospheric disturbances can reliably serve as earthquake precursors, it is imperative to rule out the influence of key external factors, specifically solar activity and geomagnetic storms, which also impact the ionosphere. To enhance the precision of seismic monitoring, it is preferable to select periods of ionospheric quiescence, during which radio signals are less affected by ionospheric perturbations.

From the data plotted in Figure 6, it can be noted that the dates of December 20th and 21st, 2015 do not indicate any appearance of seismo-ionospheric signatures, as during this period the Earth's magnetosphere experienced strong magnetic field agitation (major disturbance of the Earth's magnetosphere, Dst[6] = −155 and Kp[7] = 7+).

Conducting an extensive analysis of key indicators associated with potential disruptive space weather phenomena was essential for accomplishing the aims of our research. Specifically, we investigated the Dst and Kp geomagnetic indices, along with the F10.7[8] solar and the SSN[9] solar activity indices. Our examination revealed that throughout the studied timeframe, none of the values of these indices surpassed their respective threshold values or deviated from them. Geomagnetic storms are typically identified using a Dst threshold of −50 nT, while the onset of such storms is indicated by a Kp threshold of 5. Moreover, significant solar activity is characterized by an F10.7 threshold of 150 sfu [Tapping, 2013], and a notable level of sunspot activity.

This circumstance, marked by the lack of significant disturbances in both geomagnetic and solar activity, considerably eased our investigation of ionospheric effects related to the strong Al Hoceima-Northern Morocco earthquake (Mw 6.4, January 25th, 2016). The stable space weather environment enabled us to distinctly concentrate on the ionospheric impacts associated with the seismic activity, without the complicating factors of intense geomagnetic storms or noteworthy solar activity influencing our observations.

Also, we report that during the day of January 21st, 2016, the Al Hoceima region experienced a seismic activity of moderate magnitude (Mw = 5.1). According to the US-NOAA[10] space weather agency, this day was also prone to increase the geomagnetic activity of category G2; hence the sudden increase in the ionospheric parameter TEC has a direct link with this moderate activity of the Earth's magnetic field.

Noted that the disturbance storm time index used in this paper was provided by the World Data Center for Geomagnetism, Kyoto (http://wdc.kugi.kyoto-u.ac.jp/wdc/Sec3.html). While the planetary K-index was retrieved from the Geomagnetic Observatory Niemegk, GFZ German Research Centre for Geosciences [Matzka et al., 2021].

These observations about the temporal variations of the geomagnetic field led us to conclude that the peaks of the ionospheric total electron content values (during December 20th, 21st, 31st, 2015 and January 20th, 21st, 2016) are not

6 50 < disturbance storm time-index < −500 nanoteslas

7 (G-scale 0, quiet geomagnetic activity) 0 < K-index < 9 (G-scale 5, extreme geomagnetic storming)

8 50 < Solar radio flux < 300 sfu; where 1 solar flux units = 10^{-22} W m^{-2} Hz^{-1}

9 0 < SunSpot Number < 300

10 https://www.swpc.noaa.gov/ (National Oceanic and Atmospheric Administration)

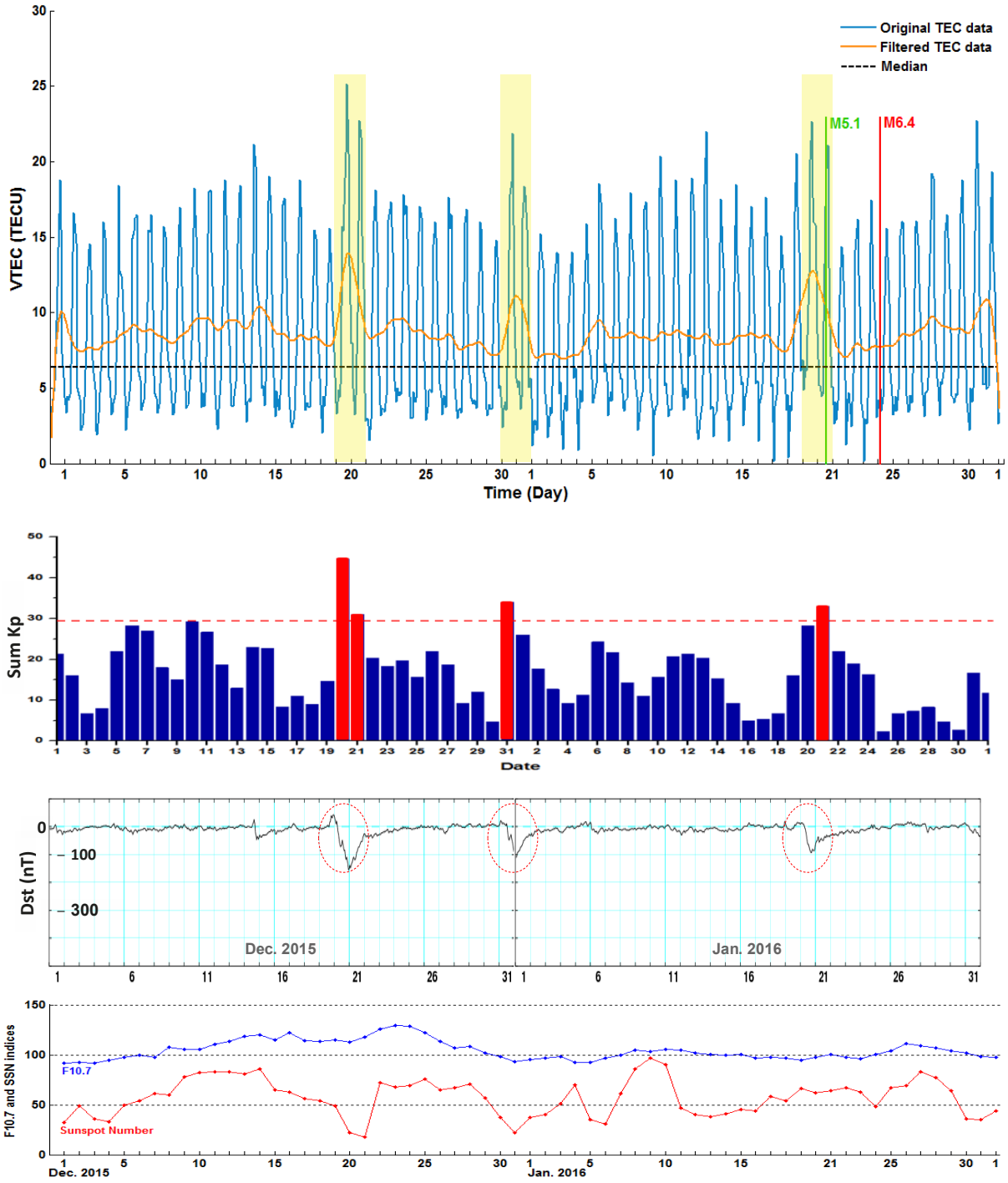

Figure 6. Top panel: Daily variations of the original and filtered ionospheric TEC (with the short-period variation removed) relative to the Al Hoceima earthquake; during the period from December 01st, 2015 to February 01st, 2016. The reference level of quiet-time TEC, established by the median value, is denoted by the horizontal black dashed line. The main earthquake date is indicated by the red vertical line. The yellow bars represent the most magnetically disturbed days (D-days), well seen in sudden changes of the disturbed storm-time index and the daily Kp-index (summation of the eight three-hourly values), displayed whit the red horizontal dashed line indicating the geomagnetic agitation threshold ($Kp \geq 5$). Bottom panel: Daily variations in the F10.7 cm radio solar emissions (blue curve) as well as the daily international Sunspot number (red curve) offer additional information on solar activity and its potential impact on the Earth's atmosphere.

related to the seismic activity, but they have a close dependence on the external physical phenomena. In addition, to remove short-period variations in the TEC data associated with diurnal variations or seasonal changes, we employed the low-pass Butterworth filter. To enhance the discernment of significant ionospheric variations potentially linked to seismic precursors, we carefully considered the selection of the filter's cutoff frequency. We chose a cutoff frequency of 0.05 Hz for the Butterworth filter guided by our intent to maintain low-frequency variations that might hold seismic relevance, while effectively attenuating high-frequency noise. This decision stems from a balanced approach that mitigates unrelated high-frequency fluctuations and accentuates noteworthy ionospheric features associated with the Al Hoceima event.

Thus, as depicted in Figure 5 and Figure 6, a very long attenuation of the ionospheric electron density can be clearly distinguished in the GPS-TEC values on the days of January 02nd-04th, 2016. During this period time, the average ionospheric TEC value is 7.12 TECU (1 TECU = 10^{16} electron/m^2), which is about four times lower than the largest TEC value recorded. To provide a sound basis for interpreting these observations, the reference level of quiet-time TEC is introduced. Represented by the horizontal black dashed line in Figure 6's top panel, this reference level is determined by the robust median value. The strategic choice of using the median ensures a reliable representation of typical ionospheric conditions and effectively mitigates the impact of outliers that could otherwise distort the interpretation of observed variations. Based on the aforementioned observations and analyses, we can confirm that these disturbances within the ionospheric layer which were triggered about twenty days before the Al Hoceima earthquake are of earth-bound nature and follow the channel transferring seismic waves of energy: Lithosphere-Neutral Atmosphere-Ionosphere. As these seismic waves radiate through the lithosphere, they simultaneously traverse the neutral atmosphere and penetrate the ionosphere. The neutral atmosphere plays a crucial intermediary role, acting as a medium that interfaces between the solid Earth and the ionosphere. The energy carried by the seismic waves serves as an impetus, setting in motion atmospheric processes that culminate in ionospheric perturbations. These perturbations manifest as fluctuations in the concentration of free electrons, consequently influencing the ionospheric TEC.

4.2 Wavelet-based diagnosis for pre-earthquake ionospheric anomalies

The wavelet analysis is used to highlight the spectral components of the signal within time series that contain non-stationary power at many different frequencies [Torrence and Compo, 1998]. The wavelet transform of function $f(x)$ associated with the mother wavelet $\varphi(x)$, it is defined as [Daubechies, 1992]:

$$Wf(\tau, s) = \frac{1}{\sqrt{s}} \int_{-\infty}^{+\infty} f(x) \varphi^* \left(\frac{x - \tau}{s} \right) dx \tag{2}$$

where $s \epsilon R^{+*}$ is a scale and $\tau \epsilon R$ is a space parameter. It measures the variation of $f(x)$ in the neighborhood of τ, whose size is proportional to s when the scale s varies from its maximum to zero, the decay of the wavelet coefficients characterizes the regularity of $f(x)$ in the neighborhood. For computational efficiency, discrete wavelet transform, which discretizes both the scale and translation parameters along a dyadic sequence, is commonly used. The sampling mechanism of the dyadic wavelet translation ensures that the numerical values are not altered due to a shift in the input TEC data. For a given φ, the corresponding reconstructing wavelet (dual) χ satisfies the condition:

$$S_{\varphi\chi,}(\omega) = \sum_{j=-\infty}^{\infty} \hat{\varphi}\left(2^j \omega\right) \hat{\chi}(2^j \omega) = 1, \qquad \forall\, \omega \epsilon R - \{0\} \tag{3}$$

where $\hat{\varphi}$ and $\hat{\chi}$ denote the Fourier transforms of φ and χ respectively. The original function $f(x)$ can be then, perfectly reconstructed from $Wf(\tau, s)$ as:

$$\sum_{j=-\infty}^{\infty} \frac{1}{2^j} Wf\left(2^j, .\right) * \chi 2^j(x) \tag{4}$$

If wavelet φ with n vanishing moments can be written as the n^{th} order derivatives of a function θ [Mallet et al., 1997], that is $\varphi = (-1)^n \theta^{(n)}$, thus the resultant wavelet transform is multiscale differential operator:

$$Wf(\tau, s) = s^n \frac{d^n}{d\tau^n}(f * \bar{\theta}_s)(u) \tag{5}$$

Suppose convolution $f * \bar{\theta}_s(u)$ averages over $f(x)$ over a domain that is proportional to scale s. Let us suppose $\varphi_1 = -\theta^1$ and $\varphi_2 = -\theta^2$ be the two wavelets defined by the above equation. Therefore $W^1 f(\tau, s)$ and $W^2 f(\tau, s)$ are two wavelet transforms of $f(x)$ smooth by smoothing $\bar{\theta}_s(u)$ from a fixed scale. Local maxima of $W^1 f(\tau, s)$ and $W^2 f(\tau, s)$ will correspond to the inflection points of $f * \bar{\theta}_s(u)$ and both correspond to a point of abrupt change in the ionospheric TEC data $f(x)$ smoothed by $\frac{1}{\sqrt{s}} g\left(\frac{x}{s}\right)$. At fine scales, the transform provides localized information of function. The modulus maxima line consists of the points that are local maxima.

The exact location of the disturbance is detected by decomposing the reconstructed ionospheric TEC data using wavelet transform. A multi-stage decomposition (MSD) based algorithm to compute DWT is proposed by Mallat [1989]. It uses a specially designed pair of finite response filters known as quadrature mirror filters (QMFs), which divide the frequency band of input TEC data into high and low-frequency components. This process repeated continuously feeding the down-sampled low-pass filter output into another identical QMF filter pair. In this way, input TEC data may be analyzed in various resolution levels corresponding to specified frequency ranges in which the TEC data is decomposed into approximation A_n and detail D_n wavelet coefficients respectively.

The frequency range of wavelet details coefficients for every DWT scale is related to TEC data sampling frequency f_s. If the sampling frequency of observed ionospheric TEC data is f_s Hz, then by Nyquist's theorem the highest frequency of its sampled version is $f_s/2$ Hz, it is the highest frequency captured in detail coefficients at scale 1. Therefore, for scale 1 the dividing point is halfway between 0 and Nyquist frequency, so the $(f_s/4 - f_s/2)$ frequency band is captured in D_1; similarly, the band captured in D_2 is $(f_s/8 - f_s/4)$ and so on.

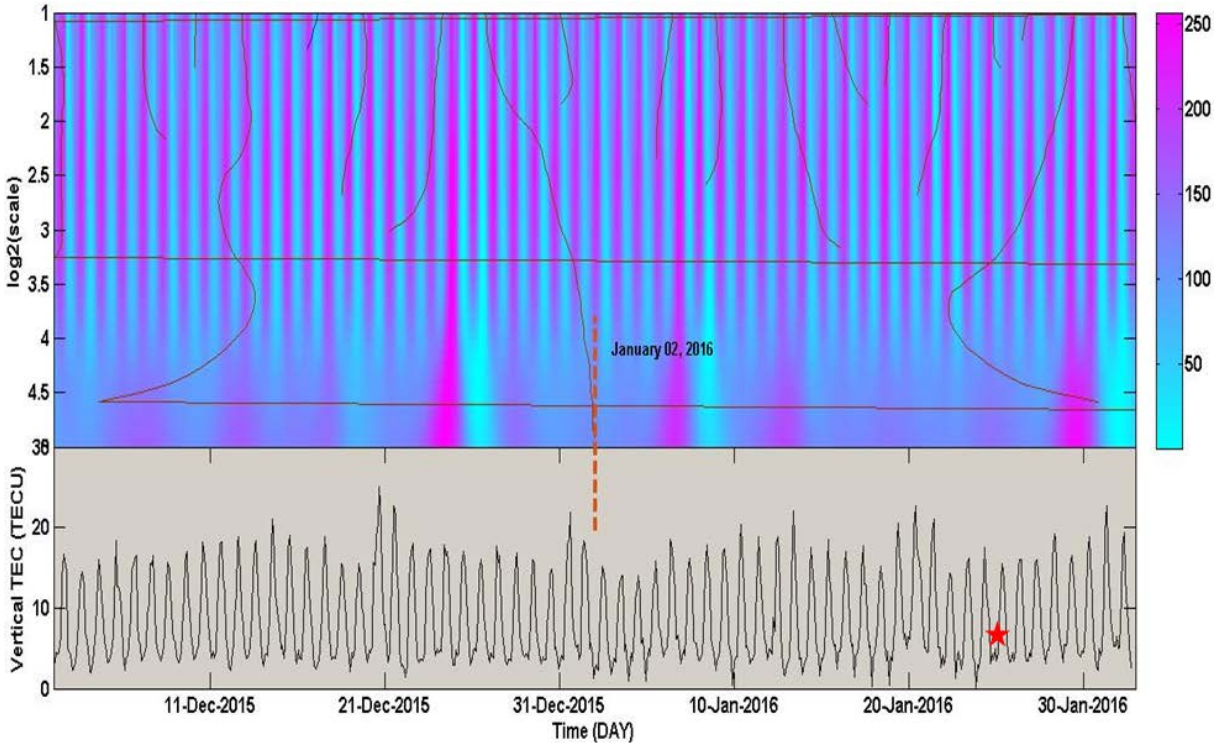

Figure 7. Variation in ionospheric GPS-TEC data (Lower panel), Wavelet transform in log scale and wavelet maxima curve (Upper panel). Period: from December 01st, 2015 to February 01st, 2016. Red star: the main Mw = 6.4 seismic event of Al Hoceima on January 25th, 2016.

Using the wavelet transform modulus maxima method, the most important information of ionospheric TEC data is carried by the position and the value of the local modulus maxima of the wavelet transform. Thus, the information carried by this method is used to detect singularities and disturbances to eliminate noise contained in the non-stationary GPS-TEC signal.

As illustrated, the lower panel of Figure 7 shows the variation in TEC data considered for the analysis of seismo-ionospheric precursors related to the 2016 Mw = 6.4 Al Hoceima earthquake event. The result of the analysis (upper panel) shows the wavelet maxima and the maximum length of the wavelet maxima curve on January 02nd, 2016, which is probably associated with the earthquake event and indicated by the dotted red line in the figure. Consequently, the sudden unexpected decreases in the GPS-TEC time series (see Fig. 6), about three weeks before the earthquake that struck the Moroccan city of Al Hoceima, were inherently seismogenic and unrelated to any space whether activities.

5. Conclusions

The present paper has focused on identifying possible seismo-ionospheric precursors in direct relation to the strong Al Hoceima-Northern Morocco earthquake (Mw 6.4, January 25th, 2016). To achieve this goal, a sample of GPS/GNSS stations was selected and used to compute local vertical TEC measurements and generate two-dimensional ionospheric TEC mapping using spherical harmonic analysis. Employing time-frequency analysis alongside the interquartile range statistical method and low-pass filtering for high-frequency variation removal from VTEC data, we propose that abrupt changes in ionospheric VTEC can serve as an initial indicator within the seismic prediction process. Therefore, our comprehensive geodetic investigation into GPS/GNSS VTEC data related to this seismic event revealed ionospheric instability over the seismoactive area of Al Hoceima. This unusual behavior in the upper ionized atmosphere occurred a few days before the main earthquake and did not correlate with extreme space weather conditions such as the eleven-year solar cycle and major disturbances of Earth's magnetosphere. These findings are consistent with recent studies focusing on ionospheric F2-layer conditions preceding moderate-to-strong earthquakes. We expect that the seismo-geodetic approach developed in this study will be a useful tool in future research, enhancing earthquake prediction capabilities through ionospheric sounding techniques enabled by advanced space-based systems.

Taking a broader perspective, the choice to consider the Al Hoceima earthquake of 2004 (Mw 6.4) holds special significance. This event offers a compelling comparative case study owing to its comparable magnitude and geographical proximity to the 2016 seismic event. By investigating TEC variations in the ionosphere prior to the 2004 event, we gain valuable context and insight into the recurring nature of ionospheric disturbances preceding seismic activity in the Al Hoceima region.

To summarize, this study provides initial evidence and new insights into the relationship between the ionosphere and seismic activity, as well as the potential for ionospheric disturbances to serve as precursors for earthquakes. However, further research is required to fully understand the mechanism behind this intricate relationship and advance a comprehensive framework for seismic prediction.

Appendix A. The International IGS Permanent Stations and the Spanish Geodetic Network of GNSS Reference Stations (ERGNSS)

Site	Longitude [degree]	Latitude [degree]	Height [m]	City	Nation
ACOR	−8.39893	43.36438	66.876	A Coruña	Spain
ALAC	−0.4812327	38.33892	60.332	Alicante	Spain
ALBA	−1.856404	38.97792	751.656	Albacete	Spain
ALME	−2.45945	36.85253	127.499	Almería	Spain
ALMO	−4.180255	38.70551	743.358	Almodóvar del Campo	Spain

Site	Longitude [degree]	Latitude [degree]	Height [m]	City	Nation
ARDU	−3.7426	41.66581	844.442	Aranda de Duero	Spain
BCLN	2.004162	41.40542	84.798	Barcelona	Spain
BOGI	21.0352111	52.4749889	139.9	Borowa Gora	Poland
BOR1	17.0734583	52.2769556	124.9	Borowiec	Poland
BRST	−4.4963889	48.3802778	65.8	Brest	France
BZRG	11.3366667	46.4988889	328.8	Bolzano – Bozen	Italy
CACE	−6.341785	39.47886	436.501	Cáceres	Spain
CANT	−3.798066	43.47198	99.245	Cantabria	Spain
CARG	−0.9738554	37.5966	57.321	Cartagena	Spain
CEBR	−4.3677778	40.4533333	775.80	Cebreros	Spain
CEU1	−5.306394	35.89197	52.447	Ceuta	Spain
COBA	−4.721111	37.9156	202.067	Córdoba	Spain
CUEN	−2.13967	40.07283	998.063	Cuenca	Spain
EBRE	0.4922222	40.8208333	107.9	Roquetes	Spain
FFMJ	8.6647222	50.0905556	178.2	Frankfurt / Main	Germany
FLRS	−31.1263889	39.4536111	79.9	Santa Cruz das Flores	Portugal
FRAG	0.3241575	41.50946	181.771	Fraga	Spain
FUER	−13.85994	28.49888	76.804	Fuerteventura	Spain
FUNC	−16.9075000	32.6477778	78.5	Funchal	Portugal
GANP	20.3229306	49.0347111	745.2	Ganovce	Slovaquie
GENO	8.9208333	44.4191667	137.0	Genova	Italy
GIRO	2.855129	42.04159	112.690	Girona	Spain
GOPE	14.7855556	49.9136111	592.6	Ondrejov	Czech Republic
GRAS	6.9205750	43.7547361	1319.3	Caussols	France
GRAZ	15.4933333	47.0669444	538.3	Graz	Austria
HERS	0.3361111	50.8672222	76.5	Hailsham	United Kingdom
HERT	0.3341667	50.8672222	83.3	Hailsham	United Kingdom
HUEG	7.5961111	47.8338889	278.4	Huegelheim	Germany
HUEL	−6.9203	37.19998	81.842	Huelva	Spain
IBIZ	1.448962	38.91125	59.857	Ibiza	Spain
IENG	7.6391667	45.0150000	316.6	Torino	Italy
IFR1	−5.10840	33.5394	1677.999991	Ifrane	Morocco
IGNE	−3.7095	40.5054	766.910	IGN–Madrid	Spain
IZAN	−16.49968	28.30807	2417.483	Izaña	Spain
JACA	−0.726528	42.56734	738.927	Jaca	Spain
JOZ2	21.0323472	52.0978333	152.5	Jozefoslaw	Poland
JOZE	21.0315333	52.0972722	141.4	Jozefoslaw	Poland
LEIJ	12.3740833	51.3539722	178.4	Leipzig	Germany

Site	Longitude [degree]	Latitude [degree]	Height [m]	City	Nation
LEON	−5.650976	42.58841	970.234	León	Spain
LPAL	−17.8938889	28.7638889	2207.0	Roque de los Muchachos	Spain
LROC	−1.2191667	46.1588889	57.9	La Rochelle	France
LUGO	−7.544686	42.99308	476.600	Lugo	Spain
MAD2	−4.2496583	40.4291611	829.5	Robledo	Spain
MADR	−4.2494444	40.4288889	829.5	Robledo	Spain
MALA	−4.393533	36.72611	119.83	Málaga	Spain
MALL	2.624551	39.55262	62.04	Palma de Mallorca	Spain
MARS	5.3537833	43.2787694	61.7	Marseille	France
MAS1	−15.6330556	27.7636111	197.3	Maspalomas	Spain
MAT1	16.7044444	40.6488889	00534.5	Matera	Italy
MATE	16.7044444	40.6488889	535.6	Matera	Italy
MELI	−2.9513889	35.2811111	93.0	Melilla	Spain
MOFR	−5.462394	37.12072	276.342	Morón de Frontera	Spain
MOLI	−1.879292	40.84124	1119.390	Molina de Aragón	Spain
MORP	−1.685497	55.21279	144.425	Morpeth	United Kingdom
MOTA	−2.870008	39.50321	779.766	Mota del Cuervo	Spain
NOT1	14.9897222	36.8758333	126.2	Noto	Italy
ONSA	11.9252778	57.3952778	45.5	Onsala	Sweden
OPMT	2.33488330	48.8358806	124.2	Paris	France
ORID	20.7940556	41.1273056	773.0	Ohrid	Macedonia
PADO	11.8960556	45.4111500	64.7	Padova	Italy
PDEL	−25.6627667	37.7477444	110.8	Ponta Delgada	Portugal
PENI	0.3589227	40.39567	108.570	Peñíscola	Spain
POTS	13.0660917	52.3792972	144.4	Potsdam	Germany
PTBB	10.4597000	52.2962000	130.2	Braunschweig	Germany
RABT	−6.8541667	33.9980556	90.1	Rabat	Morocco
REDU	5.1447222	50.0013889	369.90	Redu	Belgium
RIGA	24.033158	56.565503	34.7	Riga	Latvia
RIO1	−2.426097	42.46424	450.366	Rioja 1	Spain
SALA	−5.495864	40.94508	854.961	Salamanca	Spain
SFER	−6.2055556	36.4641667	85.8	San Fernando	Spain
SNTG	−8.551723	42.88543	312.736	Santiago	Spain
SOFI	23.3947000	42.5561000	1119.6	Sofia	Bulgaria
SONS	−3.96397	39.67535	808.944	Sonseca	Spain
SPT0	12.532884	57.425384	219.9	Boras	Sweden
SULP	24.0144861	49.8355861	370.5	Lviv	Ukraine
TALR	−5.235393	39.03508	498.909	Talarrubias	Spain

Site	Longitude [degree]	Latitude [degree]	Height [m]	City	Nation
TARI	−5.602621	36.00851	49.912	Tarifa	Spain
TERU	−1.124301	40.35050	956.167	Teruel	Spain
TLSE	1.4808333	43.5605556	207.2	Toulouse	France
TN01	−16.24116	28.47718	51.787	Santa Cruz	Spain
TN02	−16.55079	28.41825	54.475	El Puerto	Spain
TN03	−16.71852	28.04716	58.543	Los Cristianos	Spain
UZHL	22.2976000	48.6320000	232.0	Uzhgorod	Ukraine
VALE	−0.3376512	39.48083	77.559	Valencia	Spain
VICA	−3.082865	38.11763	852.442	Villacarrillo	Spain
VIGO	−8.813072	42.18398	87.761	Vigo	Spain
VILL	−3.9519444	40.4433333	647.5	Villafranca	Spain
VIS0	18.3672222	57.6536111	79.8	Visby	Sweden
WAB2	7.4642556	46.9237500	611.21	Bern	Switzerland
WROC	17.0620278	51.1132639	180.3	Wroclaw	Poland
WSRT	6.6045000	52.9146000	86.0	Westerbork	Netherlands
WTZZ	12.8789056	49.1442139	665.89	Bad Koetzting	Germany
YEB1	−3.090198	40.52378	975.336	Yebes 1	Spain
YEBE	−3.088629	40.5249	972.758	Yebes	Spain
YKRO	−5.2400000	6.8705556	270	Yamoussoukro	Ivory Coast
ZARA	−0.8821648	41.63339	296.094	Zaragoza	Spain
ZFRA	−6.410043	38.42601	587.43	Zafra	Spain
ZIMM	7.4652778	46.8769444	956.7	Zimmerwald	Switzerland

Table A1. Geographic coordinates and location of the 103 ground-based GNSS permanent stations network used for geodetic data processing.

Acknowledgements. The access to the GPS/GNSS data is acknowledged to International GNSS Service and the Estaciones de Referencia GNSS maintained by the Instituto Geográfico Nacional-Spain. The authors gratefully acknowledge the World Data Center (WDC) Kyoto, the NOAA and the German Research Centre for Geosciences (GFZ) for making the solar-geomagnetic data available. The authors would also like to thank Pr. Sergey. A. Pulinets (Space Research Institute, Russia) and Pr. Dimitar Ouzounov (Chapman Univ., USA) for their generous support and encouragement during the preparation of this manuscript.

References

Ben Sari, D. (2004). Prévision et prévention des catastrophes naturelles et environnementales : Le Cas du Maroc, Sciences de la Terre. Edition UNISCO, 234 p., ISBN 92-3-203980-X.

Bezzeghoud, M. and E. Buforn (1999). Source parameters of the 1992 Melilla (Spain, Mw = 4.8), 1994 Al Hoceima (Morocco, Mw = 5.8) and Mascara (Algeria, Mw = 5.7) earthquakes and seismotectonic implications, Bull. Seismol. Soc. Am., 89, 359-372.

Coburn, A. and R. Spence (2002). Earthquake protection, Second edition. John Wiley & Sons, Ltd. ISBN: 0-471-49614-6.

Daubechies, I. (1992). Ten lectures on wavelets, Society for Industrial and Applied Mathematics, USA. ISBN: 978-0-89871-274-2.

Dautermann, T., E. Calais, J. Haase and J. Garrison (2007). Investigation of Ionospheric Electron Content Variations before Earthquakes in Southern California, 2003-2004, J. Geophys. Res., 112, B02106, doi:10.1029/2006JB004447.

Dekking, F.M., C. Kraaikamp, H.P. Lopuhaä and L.E. Meester (2005). Exploratory data analysis: numerical summaries. In A modern introduction to probability and statistics Understanding Why and How, 231-243 Springer. ISBN: 978-1-85233-896-1.

Dobrovolsky, I.P., S.I. Zubkov and V.I. Miachkin (1979). Estimation of the size of earthquake preparation zones, Pageoph., 117, 1025-1044, https://doi.org/10.1007/BF00876083.

Hofmann-Wellenhof, B. and H. Moritz (2005). Physical geodesy, 2nd edn. Wien, ISBN 978-3-211-23584-3 SpringerWienNewYork.

Kelley, M.C. (2009). The Earth's Ionosphere: Plasma Physics and Electrodynamics, Second edition. Elsevier, ISBN 978-0-12-088425-4.

Liu, J.Y., Y.I. Chen, S.A. Pulinets, Y.B. Tsai and Y.J. Chuo (2000). Seismo-ionospheric signatures prior to $M \geq 6.0$ Taiwan earthquakes, Geophys. Res. Lett., 27, 19, 3113-3116, doi:10.1029/2000gl011395.

Liu, J.Y., Y.I. Chen, C.H. Chen, C.Y. Liu, C.Y. Chen, M. Nishihashi, J. Li, Y.Q. Xia, K.I. Oyama, K. Hattori and C.H. Lin (2009). Seismoionospheric GPS total electron content anomalies observed before the 12 May 2008 Mw7.9 Wenchuan earthquake, J. Geophys. Res., 114: A04320.

Mallat, S.G. (1989). A theory for multiresolution signal decomposition: the wavelet representation, IEEE transactions on pattern analysis and machine intelligence 11, 7, 674-693.

Mallet, Y., D. Coomans, J. Kautsky and O. De Vel (1997). Classification using adaptive wavelets for feature extraction. in IEEE Transactions on Pattern Analysis and Machine Intelligence, 19, 10, pp. 1058-1066, doi:10.1109/34.625106.

Matzka, J., C. Stolle, Y. Yamazaki, O. Bronkalla and A. Morschhauser (2021). The geomagnetic Kp index and derived indices of geomagnetic activity, Space Weather, 19, 5, https://doi.org/10.1029/2020SW002641.

Mitra, A.P. (1974). Ionospheric effects of solar flares, Springer Netherlands, Astrophysics and Space Science Library 46, ISBN: 978-94-010-2233-0.

Opio, P., F.M. D'ujanga and T. Ssenyonga (2015). Latitudinal variation of the ionosphere in the African sector using GPS TEC data, Adv. Space. Res., 55, 6, 1640-1650, doi:10.1016/j.asr.2014.12.036.

Sasmal, S., S. Chowdhury, S. Kundu, D.Z. Politis, S.M. Potirakis, G. Balasis, M. Hayakawa and S.K. Chakrabarti (2021). Pre-Seismic Irregularities during the 2020 Samos (Greece) Earthquake ($M = 6.9$) as Investigated from Multi-Parameter Approach by Ground and Space-Based Techniques, Atmosphere 12, 1059, https://doi.org/10.3390/atmos12081059.

Satti, M.S., M. Ehsan, A. Abbas, M. Shah, J.F. de Oliveira-Júnior and N.A. Naqvi (2022). Atmospheric and ionospheric precursors associated with $M_w \geq 6.5$ earthquakes from multiple satellites, J. Atmos. Sol-Terr. Phy., 227, 105802, https://doi.org/10.1016/j.jastp.2021.105802.

Sekertekin, A., S. Inyurt and S. Yaprak (2020). Pre-seismic ionospheric anomalies and spatio-temporal analyses of MODIS Land surface temperature and aerosols associated with Sep, 24 2013 Pakistan Earthquake, J. Atmos. Sol-Terr. Phy., 200, 105218, doi:10.1016/j.jastp.2020.105218.

Schaer, S. (1999). Mapping and predicting the Earth's ionosphere using the Global Positioning System, Geod.-Geophys. Arb. Schweiz., 59.

Stich, D., F.d.L. Mancilla, D. Baumont and J. Morales (2005). Source analysis of the Mw 6.3 2004 Al Hoceima earthquake (Morocco) using regional apparent source time functions, J. Geophys. Res., 110, B6, doi:10.1029/2004jb003366.

Tachema, A. and A. Nadji (2019). Geodetic contribution to predict the seismological activity of the Italian metropolis by the ionospheric variant of GPS_TEC, J. Atmos. Sol-Terr. Phy., 183, 1-10, https://doi.org/10.1016/j.jastp.2018.12.006.

Tachema, A. and A. Nadji (2020). Contribution of ionospheric TEC anomalies to detecting the seismic precursors related to the 2008 Oran-Algeria event, Adv. Space. Res., 65, 11, 2559-2572, https://doi.org/10.1016/j.asr.2020.03.007.

Tachema, A. (2022). Could the moderate-sized earthquakes trigger pre-seismic ionospheric irregularities? Study of the 2011 Murcia earthquake in the Mediterranean region (SE-Spain), EGU General Assembly 2022, Vienna, Austria, 23-27 May 2022, EGU22-1438, https://doi.org/10.5194/egusphere-egu22-1438.

Tachema, A., A. Nadji and M. Bezzeghoud (2022). Geodetic analysis for investigating possible seismo-ionospheric precursors related to the Ain Témouchent earthquake of December 22, 1999, in NW Algeria, Arab. J. Geosci., 15, 1270, https://doi.org/10.1007/s12517-022-10533-4.

Tachema, A. (2024). Identifying pre-seismic ionospheric disturbances using space geodesy: A case study of the 2011 Lorca earthquake (Mw 5.1), Spain, Earth Sci Inform., https://doi.org/10.1007/s12145-024-01272-z.

Tahayt, A., K.L. Feigl, T. Mourabit, A. Rigo, R. Reilinger, S. McClusky, A. Fadil, E. Berthier, L. Dorbath, M. Serroukh, F. Gomez and D. Ben Sari (2009). The Al Hoceima (Morocco) earthquake of 24 February 2004, analysis and interpretation of data from ENVISAT ASAR and SPOT5 validated by ground-based observations, Remote Sens. Environ., 113, 2, 306-316, doi:10.1016/j.rse.2008.09.015.

Tapping, K.F. (2013). The 10.7 cm solar radio flux (F10.7), Space Weather, 11, 7, 394-406, doi:10.1002/swe.20064.

Teunissen, P.J.G. and O. Montenbruck (Eds.) (2017). Springer Handbook of Global Navigation Satellite Systems, doi:10.1007/978-3-319-42928-1.

Thomas, J.N., J. Huard and F. Masci (2017). A Statistical Study of Global Ionospheric Map Total Electron Content Changes Prior to Occurrences of $M \geq 6.0$ Earthquakes during 2000-2014, J. Geophys. Res. Space Phys., 122, 2151-2161, doi.org/10.1002/2016JA023652.

Torrence, C. and G.P. Compo (1998). A practical guide to wavelet analysis, B. Am. Meteorol. Soc., 79, 1, 61-78, https://doi.org/10.1175/1520-0477(1998)079<0061:APGTWA>2.0.CO;2.

World Data Center for Geomagnetism, Kyoto, Nose, M., T. Iyemori, M. Sugiura, T. Kamei (2015). Geomagnetic Dst index, doi:10.17593/14515-74000.

***CORRESPONDING AUTHOR: Abdennasser TACHEMA**,
Institute of Science and Applied Techniques, Department of Science, University of Tlemcen, 13000 Tlemcen, Algeria
e-mail: tachema_abdennasser@yahoo.com; abdennasser.tachema@univ-tlemcen.dz